

1 An exhaustive survey of regular peptide 2 conformations using a new metric for 3 backbone handedness (h)

4 Ranjan V. Mannige^{1,2,*}

5 ¹ Molecular Foundry, Lawrence Berkeley National Laboratory, Berkeley, CA, U.S.A.

6 ² Present address: The Multiscale Institute, Redwood City, CA, U.S.A.

7 * ranjanmannige@gmail.com

8 ABSTRACT

9 The Ramachandran plot is important to structural biology as it describes a peptide backbone in the
10 context of its dominant degrees of freedom – the backbone dihedral angles ϕ and ψ (Ramachandran
11 *et al.*, 1963). Since its introduction, the Ramachandran plot has been a crucial tool to characterize protein
12 backbone features. However, the conformation or twist of a backbone as a function of ϕ and ψ has not
13 been completely described for both *cis* and *trans* backbones. Additionally, little intuitive understanding
14 is available about a peptide's conformation simply from knowing the ϕ and ψ values of a peptide (e.g.,
15 is the regular peptide defined by $\phi = \psi = -100^\circ$ left-handed or right-handed?). This report provides
16 a new metric for backbone handedness (h) based on interpreting a peptide backbone as a helix with
17 axial or vertical displacement d and angular displacement θ , both of which are derived from a peptide
18 backbone's internal coordinates, especially dihedral angles ϕ , ψ and ω . In particular, $h = \sin(\theta)d/|d|$ with
19 range $[-1, 1]$ and negative (or positive) values indicating left(or right)-handedness. The metric h is used
20 to characterize the handedness of every region of the Ramachandran plot for both *cis* ($\omega = 0^\circ$) and *trans*
21 ($\omega = 180^\circ$) backbones, which provides the first exhaustive survey of twist handedness in Ramachandran
22 (ϕ, ψ) space. These maps fill in the 'dead space' within the Ramachandran plot, which are regions that
23 are not commonly accessed by globular (structured) proteins, but which may be accessible to intrinsically
24 disordered proteins, short peptide fragments, and protein mimics such as peptoids. Finally, building on
25 the work of Zacharias and Knapp (2013), this report presents a new plot based on d and θ that serves
26 as a universal and intuitive alternative to the Ramachandran plot. The universality arises from the fact
27 that the co-inhabitants of such a plot include every possible peptide backbone including *cis* and *trans*
28 backbones. The intuitiveness arises from the fact that d and θ provide, at a glance, numerous aspects of
29 the backbone including compactness, handedness, and planarity.

30 INTRODUCTION

31 The backbone of a protein (Fig. 1a) can twist and turn into numerous conformations (folds), in part
32 due to the amino acid sequence that the protein displays. Understanding how a backbone twists is of
33 great importance to the field of biochemistry, since understanding the structure of a protein goes a long
34 way towards understanding how a protein functions (Alberts *et al.*, 2002; Berg *et al.*, 2010). While the
35 conformation of a peptide backbone is dependent on a number of parameters (bond lengths, bond angles,
36 and dihedral angles), Ramachandran *et al.* (1963) recognized that the twist of a peptide backbone can be
37 described to a great degree by the dihedral angles ϕ and ψ (Fig. 1a).

38 Today, two-dimensional (ϕ, ψ) plots are called Ramachandran plots (or 'maps'), and are introduced in
39 undergraduate biology textbooks as a guide for understanding a peptide backbone's general conformational
40 state or 'twistedness' at a glance (Bragg *et al.*, 1950; Pauling and Corey, 1951b; Pauling *et al.*, 1951;
41 Linderstrøm-Lang, 1952; Laskowski *et al.*, 1993; Chothia *et al.*, 1997; Hooft *et al.*, 1997; Cooper and
42 Hausman, 2013; Alberts *et al.*, 2002; Laskowski, 2003; Ho *et al.*, 2003; Eisenberg, 2003; Berg *et al.*, 2010;
43 Mannige, 2014). The Ramachandran plot is especially useful because (stable) proteins are hierarchical in
44 structure (Linderstrøm-Lang, 1952): the final (tertiary) conformation of a *structured* protein is composed
45 of discrete secondary structures – *regular* structures – that interact with each other and are strung
46 together by loops that are less regular (Alberts *et al.*, 2002; Berg *et al.*, 2010). Each regular secondary

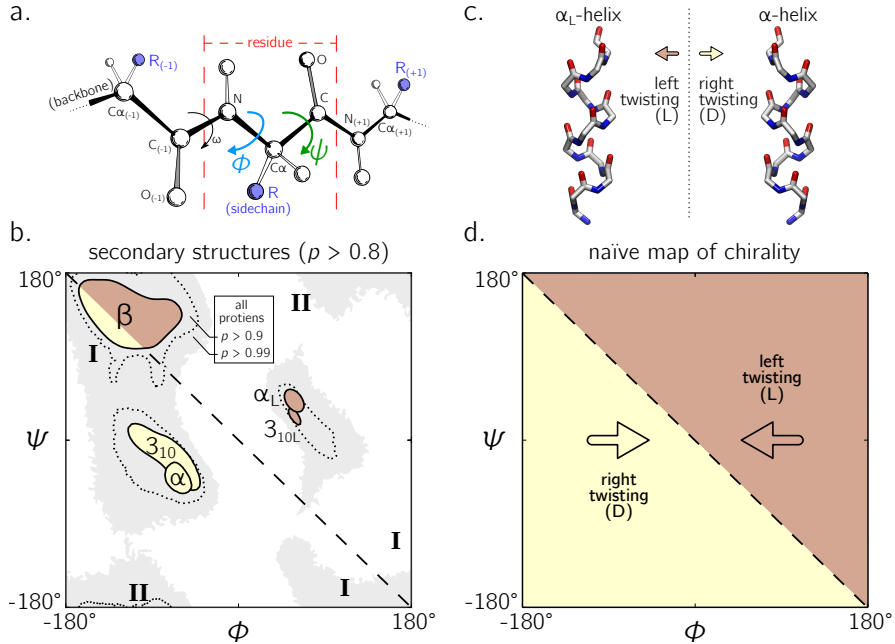


Figure 1. The backbone of a single residue (a) can be described by its dihedral angles ϕ and ψ (and in smaller part, ω , which is predominantly *trans* or $\sim 180^\circ$). For example, repeating a value for ϕ and ψ for every residue within a peptide – i.e., selecting a point on the Ramachandran plot (b) – results in regular secondary structures that then combine to form most globular proteins in the protein databank (Berman *et al.*, 2000). The twist of each perfectly regular secondary structure possesses a distinct chirality: left-handed or right-handed; examples are shown in (c). all molecular representations in this text are shown in ‘licorice’ form, with the colors red, blue and white representing the oxygen, nitrogen and carbon atoms. As evidenced in (c), the -ve diagonal within the Ramachandran plot (dashed line described by $\phi = \psi$) divides right-handed peptides from left-handed peptides, which leads to the naïve picture of handedness (d). Zacharias and Knapp (2013) showed that this picture is over simplistic, however an in-depth characterization of the backbone in all regions was not performed, and will be done here for both *cis* ($\omega = 0$) and *trans* backbones ($\omega = \pi$). Due to low count within the studied database (see Methods), the two left-handed helices in (b) are arbitrarily marked and have no statistical significance. Panel (a) is modified from Mannige *et al.* (2016).

47 structure describes a backbone whose per-residue (ϕ, ψ) values are generally the same, and therefore
48 their ‘locations’ on the Ramachandran plot act as structural landmarks (Fig. 1b).

49 So far, our understanding of the Ramachandran plot has been limited mostly to ‘structured’ proteins
50 that display stable conformations (Berman *et al.*, 2000; Alberts *et al.*, 2002). These types of proteins
51 occupy only a limited region of the plot (dotted regions in Fig. 1b). The regular backbone conformations
52 in these regions are well understood; for example, known regular structures that are to the right of
53 the negatively sloping diagonal (dashed line in Fig. 1b; henceforth denoted as the ‘-ve diagonal’) are
54 left-handed in backbone twist, while those that are to the left of the diagonal are right-handed (left- and
55 right-handed regions are respectively shaded brown and gold¹). For example, the position of the idealized
56 left- and right-handed α -helices (Fig. 1c) – respectively denoted as α_L and α in Fig. 1b – are on opposite
57 sides of the -ve diagonal. The ‘naïve view’ of handedness, obtained from looking only at structured
58 proteins, would be the expectation that the -ve diagonal neatly separates the Ramachandran plot into
59 regions of left- and right-handedness (Fig. 1d).

60 However, structured proteins represent only a fraction of functional proteins. Indeed, up to 15%
61 of mammalian proteins are completely disordered – they natively display multiple, often extended,
62 conformations (Mannige, 2014) – and up to 50% of the mammalian proteins display large (> 30 residue)
63 stretches of disorder (Iakoucheva *et al.*, 2002; Ward *et al.*, 2004; Orosz and Ovádi, 2011). Interestingly,

¹Go Hillies!

when compared to structured backbones, structurally degenerate or disordered backbones occupy many more regions within the Ramachandran plot (Beck *et al.*, 2008).

Additionally, a number of peptide mimics – especially peptoids (Sun and Zuckermann, 2013) – display novel secondary structures that occupy regions that are strictly disallowed by proteins due to steric clashes. For example, a ‘higher-order’ peptoid secondary structure – the Σ -strand (Mannige *et al.*, 2015; Robertson *et al.*, 2016) – samples regions of the Ramachandran plot (‘I’ in Fig. 1b) that are not permitted within natural proteins (this is because of the lack of backbone hydrogen bond donors in peptoids). Another secondary structure – the ‘ ω -strand’ (Gorske *et al.*, 2016) – samples similarly historically uncharted regions of the Ramachandran plot (‘II’ in Fig. 1b). Importantly, backbone twist handedness plays a crucial part in explaining these new motifs: as one goes along the backbones of these secondary structures, alternating residues occupy equal but opposite backbone twists [for this reason, the Σ -strand is relatively linear, albeit meandering; Mannige *et al.* (2015); Mannige *et al.* (2016)].

Despite these recent discoveries of natively disordered proteins and novel peptidomimetic structures, a complete understanding of backbone conformations that stray from the ‘structured’ regions on the Ramachandran plot is missing, which impedes our ability to identify and explore such conformations. Towards filling this gap in understanding, this report outlines a detailed study of how regular backbones twist in every region of the Ramachandran plot. In particular, this report develops and explores a new metric for handedness (h) based on modeling a regular backbone (described below) as a helix (Shimanouchi and Mizushima, 1955; Miyazawa, 1961; Zacharias and Knapp, 2013). The metric is used to exhaustively chart the handedness of regular backbones in every region of the Ramachandran plot. In doing so, this survey provides a new graphical format to explore new types of secondary structures being discovered (Mannige *et al.*, 2015; Gorske *et al.*, 2016), while dispelling the naïve view of handedness (Fig. 1d) by showing that the distribution of handedness as a function of ϕ and ψ is more complicated than the distribution allowed by the naïve view. The results also show that the Ramachandran plot whose ϕ and ψ values range between 0° and 360° is more intuitive and visually meaningful (compared to those that range between -180° and 180°), particularly for *cis* backbones. Finally, this work builds on a previous report (Zacharias and Knapp, 2013) and helps complete our understanding of the ways in which a peptide backbone twists, which is a basic component of structural biology.

METHODS

While angular units in this report switch between radians and degrees, their units in any particular situation may be inferred by the presence or absence of the degree symbol ($^\circ$). All methods and materials required to produce this manuscript are freely available at https://github.com/ranjanmannige/backbone_chirality.

Deriving measures for backbone handedness

Numerous metrics for molecular chirality and handedness have so far been discussed (Harris *et al.*, 1999). For example, metrics for chirality have been introduced that focus on vector orientations (Kwiecińska and Cieplak, 2005; Kabsch and Sander, 1983; Gruziel *et al.*, 2013), optical activity (Osipov *et al.*, 1995), and molecular shape (Ferrarini and Nordio, 1998). However, this report will focus on a simpler metric for chirality associated with an idealized helix within which all (regular) backbone atoms of one type sit (Shimanouchi and Mizushima, 1955; Miyazawa, 1961; Zacharias and Knapp, 2013). Here, a ‘regular’ backbone indicates that each tunable parameter within a unit or ‘residue’ – say a particular dihedral angle – remains the same for all residues. Below, regular backbones are modeled in context of helical parameters that, when combined, form an intuitive metric for backbone handedness.

Describing a regular backbone as a helix

Interest in how a backbone may be represented as a helix emerged shortly after the first secondary structures were introduced (Pauling *et al.*, 1951; Pauling and Corey, 1951b,a). In particular, Shimanouchi and Mizushima (1955) had derived a set of equations that fit a platonic helix to the atoms within a regular backbone. While the formalisms described by Shimanouchi and Mizushima (1955) [and later on by Miyazawa (1961), discussed below] apply to repeating linear polymers of arbitrary complexity, this report focuses specifically on how peptides may be modeled. Fig. 2 describes an arbitrary peptide backbone that may be represented either using internal coordinates (*i*) or helical coordinates (*ii*).

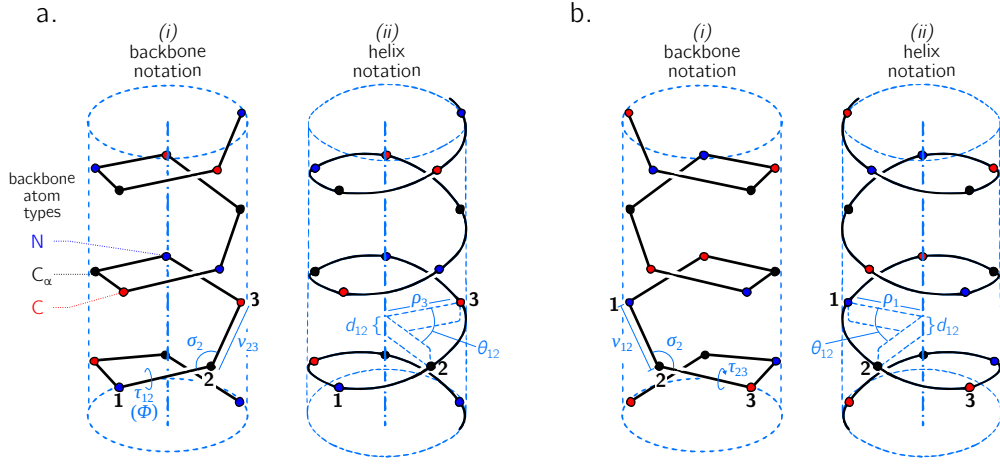


Figure 2. Internal coordinate (i) and helical coordinate (ii) representations of right-handed (a) and left-handed (b) regular backbones. Internal coordinates are a function of bond lengths (e.g., v_{12}), angles (σ_2), and dihedral angles (τ_{12}), while helical coordinates are a function of displacement along the helical axis (d_{12}), angular displacement in the plane perpendicular to the helical axis (θ_{12}) and shortest distance of an atom of type i from the helical axis (ρ_i). Representations are derived from Figs. 1 and 2 in Shimanouchi and Mizushima (1955).

115 Internal coordinates are associated with stereochemical terms: bond lengths (v_{ij}) between adjacent
 116 atoms i and j , bond angles (σ_i) between the two backbone bonds adjacent to atom i , and dihedral or
 117 torsion angles (τ_{ij}), which are associated with the bond $i - j$ and the atoms preceding and succeeding
 118 these atoms. Helical coordinates (Fig. 2(ii)) are described using measures of vertical displacement (d ; this
 119 is related to the pitch of a platonic helix), angular displacement (θ) and the radius of the helix (ρ_i) that
 120 hosts all backbone atoms of type i . Therefore, the single cylinder shown in Fig. 2 is too simplistic as there
 121 should be one distinct cylinder or radius per atom type.

122 Given that there are three atoms associated with a residue (Fig. 1a), $d = d_{n,\alpha} + d_{\alpha,c} + d_{c,n}$ and
 123 $\theta = \theta_{n,\alpha} + \theta_{\alpha,c} + \theta_{c,n}$. Here, $d_{i,j}$ and $\theta_{i,j}$ respectively refer to the vertical and angular displacement
 124 between adjacent atoms i and j . Subscripts ‘ n ’, ‘ α ’, and ‘ c ’ respectively refer to the backbone nitrogen,
 125 α -carbon and carbonyl carbon atoms (Fig. 1a). The notation used by Shimanouchi and Mizushima (1955)
 126 was in terms of matrices, which were then simplified by Miyazawa (1961) into trigonometric terms. In
 127 particular, Miyazawa (1961) noted that the total residue-residue vertical displacement (d) and angular
 128 displacement (θ) may be retrieved using the following two equations.

$$\begin{aligned} \cos\left(\frac{\theta}{2}\right) = & \cos\left(\frac{+\phi + \psi + \omega}{2}\right) \sin\left(\frac{\sigma_n}{2}\right) \sin\left(\frac{\sigma_\alpha}{2}\right) \sin\left(\frac{\sigma_c}{2}\right) \\ & - \cos\left(\frac{+\phi - \psi + \omega}{2}\right) \sin\left(\frac{\sigma_n}{2}\right) \cos\left(\frac{\sigma_\alpha}{2}\right) \cos\left(\frac{\sigma_c}{2}\right) \\ & - \cos\left(\frac{+\phi + \psi - \omega}{2}\right) \cos\left(\frac{\sigma_n}{2}\right) \sin\left(\frac{\sigma_\alpha}{2}\right) \cos\left(\frac{\sigma_c}{2}\right) \\ & - \cos\left(\frac{-\phi + \psi + \omega}{2}\right) \cos\left(\frac{\sigma_n}{2}\right) \cos\left(\frac{\sigma_\alpha}{2}\right) \sin\left(\frac{\sigma_c}{2}\right) \end{aligned} \quad (1)$$

$$\begin{aligned}
d \sin\left(\frac{\theta}{2}\right) = & (+v_{n,\alpha} + v_{\alpha,c} + v_{c,n}) \sin\left(\frac{+\phi + \psi + \omega}{2}\right) \sin\left(\frac{\sigma_n}{2}\right) \sin\left(\frac{\sigma_\alpha}{2}\right) \sin\left(\frac{\sigma_c}{2}\right) \\
& - (+v_{n,\alpha} - v_{\alpha,c} + v_{c,n}) \sin\left(\frac{+\phi - \psi + \omega}{2}\right) \sin\left(\frac{\sigma_n}{2}\right) \cos\left(\frac{\sigma_\alpha}{2}\right) \cos\left(\frac{\sigma_c}{2}\right) \\
& - (+v_{n,\alpha} + v_{\alpha,c} - v_{c,n}) \sin\left(\frac{+\phi + \psi - \omega}{2}\right) \cos\left(\frac{\sigma_n}{2}\right) \sin\left(\frac{\sigma_\alpha}{2}\right) \cos\left(\frac{\sigma_c}{2}\right) \\
& - (-v_{n,\alpha} + v_{\alpha,c} + v_{c,n}) \sin\left(\frac{-\phi + \psi + \omega}{2}\right) \cos\left(\frac{\sigma_n}{2}\right) \cos\left(\frac{\sigma_\alpha}{2}\right) \sin\left(\frac{\sigma_c}{2}\right)
\end{aligned} \quad (2)$$

129 The ranges for d and θ , respectively, are $[-\lambda, +\lambda]$ and $[0, 2\pi]$ (the positive limit λ is defined by allowed
130 values for the various internal coordinates). As above, subscripts ‘n’, ‘ α ’, and ‘c’ respectively refer to
131 the backbone nitrogen, α -carbon and carbonyl carbon atoms; v_{ij} refers to the distance between adjacent
132 atoms i and j ; σ_i refers to the angle between the adjacent bonds that have i as the common atom. The
133 dihedral angles ϕ , ψ , and ω represent the traditional symbols for backbone dihedral angles, which may
134 be otherwise denoted as $\tau_{n,\alpha}$, $\tau_{\alpha,c}$, and $\tau_{c,n(+1)}$, respectively.

Finally, for any type of atom (say α -carbons), the radius or distance from the helical axis ρ_α is defined by

$$\begin{aligned}
2\rho_\alpha^2 [1 - \cos(\theta)] + d^2 = & v_{\alpha,c}^2 + v_{c,n}^2 + v_{n,\alpha}^2 - 2v_{c,n} [v_{\alpha,c} \cos(\sigma_c) + v_{n,\alpha} \cos(\sigma_n)] \\
& + 2v_{\alpha,c} v_{n,\alpha} [\cos(\sigma_c) \cos(\sigma_n) - \sin(\sigma_c) \sin(\sigma_n) \cos(\tau_{c,n})]
\end{aligned} \quad (3)$$

Miyazawa (1961) noted that the right-hand side of Eqn. 3 is also the squared distance between adjacent atoms of the same type (denoted here as d_α^2 for α -carbons), which allows for a more simplified form

$$\rho_\alpha = \sqrt{\frac{d_\alpha^2 - d^2}{2 - 2 \cos(\theta)}} \quad (4)$$

135 The distance between adjacent α -carbons (d_α) is $\sim 3.8\text{\AA}$ for *trans* peptides and $\sim 3.2\text{\AA}$ for *cis* peptides.
136 Other radii (ρ_c, ρ_n) can be obtained by cycling through (α, c, n) subscripts within Eqns. 3 and 4². Note
137 that all ρ_i 's are functions of θ, d (along with other internal coordinates), and so one may use two of
138 the three terms (d, θ, ρ_i) – to describe the helical state of a peptide. Since there is only one d and θ per
139 backbone (compared to three ρ_i 's, one per atom type), this report utilizes d and θ as the two descriptors
140 [discussions on this choice have also been made by Zacharias and Knapp (2013)].

Eqns. 1 and 2 may be substantially simplified (Miyazawa, 1961), given that backbone bond lengths and angles are much less ‘tunable’ when compared to dihedral angles (Ramachandran *et al.*, 1963; Imrota *et al.*, 2015a; Esposito *et al.*, 2013; Imrota *et al.*, 2015b). In particular, most backbone bond lengths and angles display one equilibrium value (Imrota *et al.*, 2015a; Esposito *et al.*, 2013; Imrota *et al.*, 2015b), while the backbone dihedral angles ϕ and ψ occupy a range of possible values and minima, e.g., regions in the Ramachandran plot that describe α -helices and β -sheets (Fig. 1b). With this in mind, Miyazawa (1961) set $\omega = \pi$ (*trans*) and substituted average (equilibrium) values for bond angles and lengths into Eqns. 1 and 2 to arrive at a simpler equation for *trans* backbones. Zacharias and Knapp (2013) published an updated version of this set of equations, which follows³.

$$\cos\left(\frac{\theta}{2}\right) = -0.8235 \sin\left(\frac{\phi + \psi}{2}\right) + 0.0222 \sin\left(\frac{\phi - \psi}{2}\right), \quad (5)$$

$$d \sin\left(\frac{\theta}{2}\right) = 2.9986 \cos\left(\frac{\phi + \psi}{2}\right) - 0.6575 \cos\left(\frac{\phi - \psi}{2}\right). \quad (6)$$

This equation is especially relevant to peptides as they occur predominantly in *trans* conformations ($\omega = \pi$). However, given the prevalence of *cis* backbones in peptide mimics such as peptoids (Mirijanian

² ρ_c and ρ_n are obtained by the following subscript conversions: ($\alpha \rightarrow c, c \rightarrow n, n \rightarrow \alpha$) and ($\alpha \rightarrow n, c \rightarrow \alpha, n \rightarrow c$).

³Values used here are also used by Zacharias and Knapp (2013). These values are:

$v_{n,\alpha} = 1.459\text{\AA}$, $v_{\alpha,c} = 1.525\text{\AA}$, $v_{c,n(+1)} = 1.336\text{\AA}$, $\sigma_\alpha = 111.0$, $\sigma_c = 117.2^\circ$, and $\sigma_n = 121.7^\circ$.
For reference, Miyazawa (1961) originally used the following values:

$v_{n,\alpha} = 1.470\text{\AA}$, $v_{\alpha,c} = 1.530\text{\AA}$, $v_{c,n(+1)} = 1.320\text{\AA}$, $\sigma_\alpha = 110.0$, $\sigma_c = 114.0$, and $\sigma_n = 123.0$.

et al., 2014; Gorske *et al.*, 2016), for completeness, the corresponding relationships for a *cis* ($\omega = 0$) backbone follows.

$$\cos\left(\frac{\theta}{2}\right) = 0.4052 \cos\left(\frac{\phi + \psi}{2}\right) - 0.4932 \cos\left(\frac{\phi - \psi}{2}\right), \quad (7)$$

$$d \sin\left(\frac{\theta}{2}\right) = 2.3093 \sin\left(\frac{\phi + \psi}{2}\right) + 0.0028 \sin\left(\frac{\phi - \psi}{2}\right). \quad (8)$$

Note that Eqns. 5 through 8 are simplifications of Eqns. 1 and 2, and are therefore prone to some limitations that are not present in Eqns. 1 and 2. For example, bond lengths (Impronta *et al.*, 2015a) and bond angles (Esposito *et al.*, 2013; Impronta *et al.*, 2015b) display some dependence on local backbone conformation. These subtle variations have great implications when dealing with a large number of residues, especially when considering bond angles. For example, when attempting to recreate a protein conformation from an original conformation's ϕ and ψ values (ignoring deviations in ω , bond angles, and lengths), the original and recreated conformations tend to deviate dramatically due to an accumulation of errors [by up to 22 Å in root mean squared deviation; Tien *et al.* (2013)]. However, when studying changes in conformationally regular and *local* stretches of peptides, such deviations are not likely to change relevant features such as handedness and extent of twistedness. If circumstances indicate that the backbone values for bond angles and ω of the peptide may be strained from their equilibrium values (e.g., due to bulky sidechains), only Eqns. 1 and 2 can be expected to faithfully (and perfectly) represent backbone features such as handedness of twist. However, the approximations of Eqns. 5 through 8 are sufficient for the purposes of this report, given that this report primarily discusses features within platonic regular backbones.

On the one-to-one correspondence between $[\phi, \psi, \omega]$ and $[d, \theta]$

Given a particular value of ω , every $[\phi, \psi]$ pair points to exactly one $[d, \theta]$. However, when using Eqns. 1 and 2, one value of ω can not be replaced with a *periodically equivalent* version of ω . For example, using $\omega = x + 2\pi$ instead of $\omega = x$ will maintain the magnitude of d and θ , but the signs will not remain conserved. This is because every summand in Eqns. 1 and 2 contains either a sine or cosine of $[\pm\phi \pm \psi \pm \omega]/2$. The issue arises because of the '2': even though the angle x is considered to be equivalent to the angle $x + 2\pi$, and even though $\cos(x + 2\pi)$ equals $\cos(x)$ (due to angle periodicity), $\cos([x \pm 2\pi]/2) = \cos(x/2 \pm \pi) = -\cos(x/2)$ (note the negative sign). Similarly, $\sin([x \pm 2\pi]/2) = -\sin(x/2)$. Therefore, even though the angles ω and $\omega + 2\pi$ may be considered to be equivalent angles, expressions such as $\cos([x - \omega + 2\pi]/2)$ and $\cos([x - \omega]/2)$ are only equal in magnitude and not in sign. I.e., one-to-one correspondence between $[\phi, \psi]$ and $[d, \theta]$ is only possible if one insists on specific values for ω s. For this reason, this report proposes to wrap the value of an amide backbone ω' between $[\Delta, \Delta + 360^\circ]$ using

$$\omega = (\omega' - \Delta)\%360 + \Delta, \quad (9)$$

where $\%$ represents the modulus function, and Δ describes the start of the range. Choosing $\Delta = -90^\circ$ would ensure that the distribution of both *cis* ($\omega = 0 \pm 20^\circ$) and *trans* ($\omega = 180 \pm 20^\circ$) will remain contiguous. Using this system, *cis* and *trans* backbones are respectively represented by $\omega = 0$ (and not 2π) and $\omega = \pi$ (not $-\pi$) for *trans* backbones. The rest of this report assumes these values of ω for *cis* and *trans* backbones.

These points lead to the conclusion that a *strict* one to one-to-one correspondence between (ϕ, ψ, ω) and (d, θ) does not exist, since multiple sets of the former may be backmapped from the latter (by reconfiguring Eqns. 1 and 2). Yet, a one-to-one correspondence may be ensured by discarding as solutions all but the one set of (ϕ, ψ, ω) , whose ω does not change after being wrapped by Eqn. 9.

Introducing an equation for backbone handedness

The helical parameters d and θ host a wealth of information, some of which is discussed in the Results section. For the purpose of developing an equation for backbone handedness, it is only important to recognize, as was done before (Zacharias and Knapp, 2013), that θ and d together are instrumental in describing backbone handedness.

The relationship between d , θ and handedness is shown in Fig. 3. While θ indicates the extent to which a regular backbone curves along a helical path, the handedness of a backbone is dependent on both

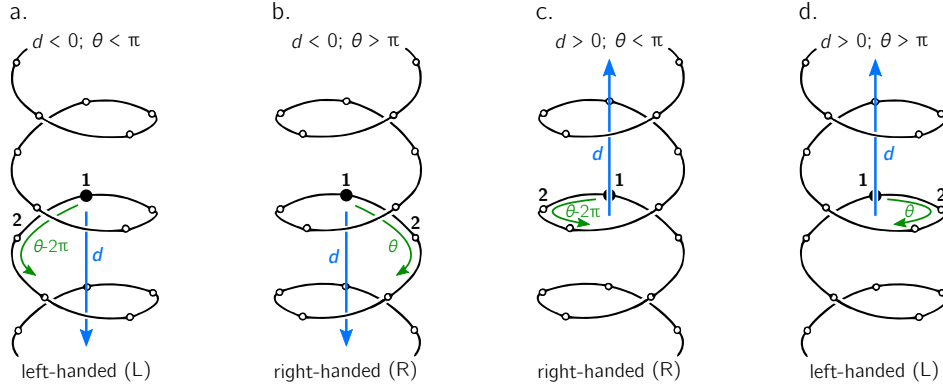


Figure 3. The handedness of a helix is a function of angular displacement perpendicular to the helical axis (θ ; green curved arrows) and linear displacement along the helical axis d (blue, vertical arrows). Note that left- and right-handed backbone twists are respectively associated with the L and D chiralities within the Fisher Projection system and S and R chiralities within the Cahn–Ingold–Prelog system (Cross and Klyne, 2013); however, as discussed in the Methods section, this report makes a distinction between helix handedness and molecular chirality.

173 θ and d . This is because the sign of d provides a frame of reference for interpreting θ . In particular, if d is
 174 negative, then $0 < \theta < \pi$ indicates left-handedness (Fig. 3a), while $\pi < \theta < 2\pi$ indicates a right-handed
 175 helix (Fig. 3b). However, if d is positive, then the manner in which the helix is ‘built’ reverses, and
 176 $0 < \theta < \pi$ indicates right-handedness (Fig. 3c), while $\pi < \theta < 2\pi$ indicates left-handedness (Fig. 3d).

These relationships allow for a simple metric for backbone handedness that depends on the sign of d and the value of θ :

$$h = \frac{d}{|d|} \sin(\theta). \quad (10)$$

177 Here, $h \in \{-1, \dots, 1\}$ is negative (or positive) when the overall twist of the backbone is left(or right)-
 178 handed. Note that $d/|d|$ is related to the traditional sign function $\text{sgn}(d)$, but deviates at $d = 0$, where
 179 the former term is undefined while the latter term is 0. Additionally, h will equal 0 if $d = 0$ or if $\theta = x\pi$
 180 (where x is an integer); for more on the meaning of d and θ in context of handedness and peptide geometry,
 181 please refer to the Results and Discussions section and Fig. 4 in particular.

182 Alternative measures of handedness

Two estimates for chirality, χ_1 and χ_2 , used to validate the new measure of handedness h (Eqn. 10), were previously used by Kwiecińska and Cieplak (2005) and Kabsch and Sander (1983), respectively. The equations are:

$$\chi_1 = \frac{1}{N} \sum_{i=2}^{N-2} \frac{(\mathbf{v}_{i-1} \times \mathbf{v}_i) \cdot \mathbf{v}_{i+1}}{v_{i-1} v_i v_{i+1}}, \quad (11)$$

$$\chi_2 = \frac{1}{N} \sum_{i=2}^{N-2} \arctan2(v_i \mathbf{v}_{i-1} \cdot \mathbf{v}_i \times \mathbf{v}_{i+1}, \mathbf{v}_{i-1} \times \mathbf{v}_i \cdot \mathbf{v}_i \times \mathbf{v}_{i+1}). \quad (12)$$

183 Here, N is the peptide length, i is the peptide residue number and the position of each α -carbon is
 184 \mathbf{N}_i , with vector $\mathbf{v}_k \equiv \mathbf{N}_{k+1} - \mathbf{N}_k$. The scalar component of the vector \mathbf{v}_i is denoted as v_i . Eqn. 11 has
 185 range $[-1, 1]$. Eqn. 12, also used by Gruziel *et al.* (2013), is the dihedral angle associated with the four
 186 contiguous α -carbons (one preceding and two succeeding the residue i), and ranges between $[-\pi, \pi]$
 187 radians. For both metrics, values deviating more from 0 are more chiral (or ‘twisted’ or ‘handed’), and
 188 left-handed twists are negative while right-handed twists are positive. Only α -carbon atom positions are
 189 used for the calculation.

Finally, a more backbone-agnostic metric of chirality has been introduced by Solymosi *et al.* (2002), which is replicated here purely for completeness:

$$\chi_3 = \frac{4!}{3N^4} \sum_{i,j,k,l \in N} \frac{((\mathbf{v}_{ij} \times \mathbf{v}_{kl}) \cdot \mathbf{v}_{il})(\mathbf{v}_{ij} \cdot \mathbf{v}_{jk})(\mathbf{v}_{jk} \cdot \mathbf{v}_{kl})}{(\mathbf{v}_{ij} \cdot \mathbf{v}_{jk} \cdot \mathbf{v}_{kl})^2 v_{il}}. \quad (13)$$

¹⁹⁰ χ_3 , of arbitrary range, is known as the chirality index G_{0S} in Solymosi *et al.* (2002) and Neal *et al.* (2003).
¹⁹¹ (i, j, k, l) are exhaustive permutations of $\{1, 2, \dots, N\}$. This metric qualitatively matches the values of
¹⁹² Eqns. 11 and 12, and, while not shown, the relationship between (ϕ, ψ) and χ_3 is available in the online
¹⁹³ GitHub repository.

194 Backbone structure generation

¹⁹⁵ The metric h (Eqn. 10) is purely analytical and does not need structures to be computationally generated,
¹⁹⁶ since Eqns. 5 through 8 that provide d and θ require only pairs of ϕ and ψ angles. However, if values
¹⁹⁷ for bond angles, lengths and dihedral angles are expected to deviate greatly from equilibrium values, θ
¹⁹⁸ and d can only be obtained from the more detailed Eqns. 1 and 2, whose parameters would likely be
¹⁹⁹ obtained from a structure. On the other hand, as χ_1 (Eqn. 11) and χ_2 (Eqn. 12) work explicitly with atom
²⁰⁰ positions, these metrics explicitly need the generation of structures. In order to use these metrics, peptides
²⁰¹ (poly-glycines) of arbitrary length were generated using the Python-based PeptideBuilder library (Tien
²⁰² *et al.*, 2013). Analysis was performed using BioPython (Cock *et al.*, 2009) and Numerical Python (Van
²⁰³ Der Walt *et al.*, 2011). Ramachandran plots that describe chirality (e.g., Fig. 5a) were generated using a
²⁰⁴ grid spacing (in degrees) of $\phi, \psi \in \{-180, -178, \dots, 178, 180\}$.

205 Backbone chirality \neq backbone handedness

²⁰⁶ Finally, it is important to recognize the distinction between backbone (twist) handedness and backbone
²⁰⁷ (molecular) chirality. Naïvely, chirality is a simple concept: a molecular conformation is achiral if its
²⁰⁸ mirror image can be superimposed onto itself, otherwise that conformation is chiral (Gold *et al.*, 1997)
²⁰⁹ (alternatively, and less commonly, achiral molecules possess inversion centers). Despite this intuitive
²¹⁰ definition, chirality has remained a confusing concept ever since its introduction (Bentley, 2010; Wallentin
²¹¹ *et al.*, 2009), which is possibly due to the fact that ‘context’ is very important when discussing chirality
²¹² (Mislow, 2002). For example, when looking at a peptide at the residue or ‘local’ level, every amino
²¹³ acid (excepting glycine) is chiral due to the presence of a chiral α -carbon (its mirror image can not be
²¹⁴ superimposed onto itself). Yet, at the macromolecular level, even an all-glycine (and therefore locally
²¹⁵ achiral) peptide will display *conformations* that are not superimposable onto each other, and so such
²¹⁶ conformations would be chiral. Alternatively, when considering handedness, if a backbone is completely
²¹⁷ flat (say, a ring, where $d = 0$), handedness (h) will be undefined, and so one can not speak of handedness
²¹⁸ of the twist. Yet, the backbone may still remain chiral; e.g., cisplatin and transplatin are planar molecules
²¹⁹ that are nonetheless chiral opposites (Testa, 2013). It is for this reason that this report chooses to be
²²⁰ careful to not claim that Eqn. 10 is a metric for peptide/backbone chirality, but of peptide backbone *twist*
²²¹ handedness. However, estimates for backbone chirality (e.g., Eqns. 11 and 12) may be used as surrogates
²²² for twist chirality to validate h (Eqn. 10), as both are related but not the same.

223 Obtaining secondary structure statistics

²²⁴ Statistics about secondary structures – particularly α -helices, 3_{10} -helices and β -sheets – used in Figs. 1b
²²⁵ and 9 were identified using the DSSP algorithm (Kabsch and Sander, 1983), although the STRIDE
²²⁶ algorithm (Frishman and Argos, 1995) provides qualitatively identical distributions. This algorithm was
²²⁷ applied to a database of 13,760 three-dimensional protein conformations (one domain per conformation)
²²⁸ with lower than 40% sequence identity, obtained from the Structural Classification of Proteins or SCOPe
²²⁹ website [Release 2.06; Fox *et al.* (2014)]. This database is currently available as: <http://scop.berkeley.edu/downloads/pdbstyle/pdbstyle-sel-gs-bib-40-2.06.tgz>.

231 RESULTS AND DISCUSSION

232 Relevance of θ and d

²³³ When discussing peptide backbones, two possible definitions of backbone ‘flatness’ (or linearity) are
²³⁴ possible: flatness at a residue level and flatness at the atomic level. In the former, all atoms of the same *type*

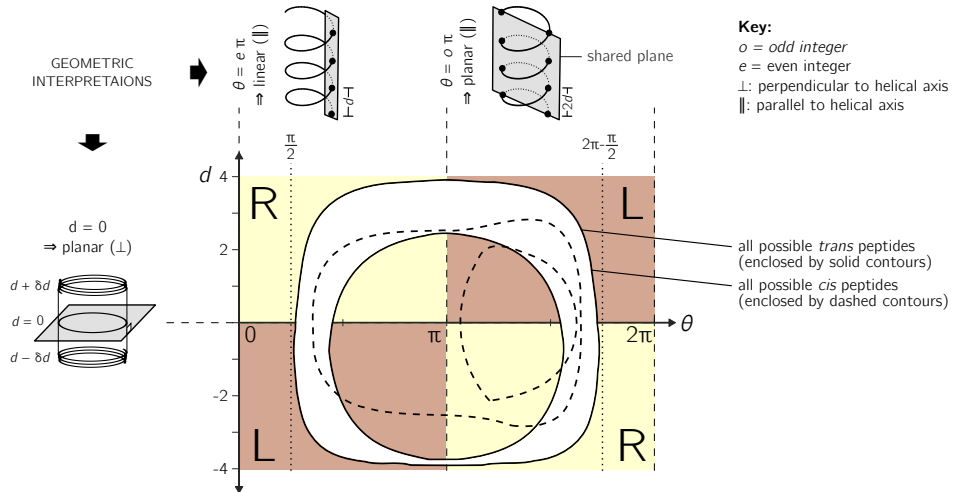


Figure 4. Further discussion on the meaning of d and θ . As shown in Fig. 3, axial separation d and angular separation θ between adjacent atoms of the same type combine to define handedness. The shaded regions within the graph show the distribution of handedness as a function of d and θ . The relevant boundaries – $\theta = x\pi$ (where x is a non-negative integer) and $d = 0$ – separate the map into four quadrants of left- and right-twisting backbones ('L' and 'R', respectively). Geometric interpretations of various boundaries, discussed in the text, are shown to the top and left of the graph. The toroid enclosed by two solid lines (and shaded white) represents all possible conformations for *trans* peptides ($\omega = 180 \pm 10^\circ$). Similarly, the region allowed for *cis* peptides are bound by the two dashed contours. As expected, *trans* and *cis* peptides behave very differently, further predicated the need to explore the two types of backbones as distinct.

are coplanar (examples of atom types are the backbone nitrogens, carbonyl carbons, α -carbons, or even sidechain β -carbons). In the latter, *all* atoms within the backbone are coplanar. For the discussions below, the former definition is chosen as the relevant scope for flatness (and ‘linearity’), as residue-by-residue behavior of the peptide is of primary relevance.

As described in Fig. 3, the helical parameters d and θ respectively refer to a vertical displacement along the helical axis and an angular displacement in a plane perpendicular to the helical axis. For example, $d = 0$ indicates a helix flattened along its helical axis (Fig. 4). This means that all regular peptides with $d = 0$ will be ring-like at some peptide length (shown in a following figure for a range of peptides). As expected from Eqn. 10, at $d = 0$, one can not tell how the helix was built, since coplanar peptides can not be described as either left- or right-twisting. Therefore, even though $d = 0$ indicates highly twisted peptides, these twists do not possess handedness. This shows up in the h metric because, at $d = 0$, $d/|d|$ is undefined.

Additionally Fig. 4 describes two important values for θ : $e\pi$ and $o\pi$, where e and o are even and odd non-negative integers. In particular, for any d , $\theta = e\pi$ indicates zero angular displacement along the axis, which puts all atoms of the same type on the same line parallel to the helical axis (Fig. 4). Similarly, $\theta = o\pi$ indicates that every alternate atom (of the same type) along the backbone will be linear, and every adjacent atom will be diametrically opposite to each other (Fig. 4); i.e., $\theta = o\pi$ indicates that all atoms of the same type will lie on a plane that is parallel to the helical axis. In short, $\theta = 0$ codes for backbones that are linear (optimally extended for a fixed d) and $\theta = \pi$ describe peptides that zig-zag along a plane perpendicular to the helical axis (for a fixed d). Finally, as evident in Fig. 4, $\theta = e\pi$ conformations are not available for peptide backbones; in these situations, $\theta = o\pi$ (e.g., π or 180°) will be the most extended type of backbone (for a fixed d). These relationships show how, *a priori*, the curve of a backbone with particular (d, θ) may be interpreted.

Finally, θ may serve as an important single-number metric for describing backbone configurations. Mannige *et al.* (2016) developed one such number – a Ramachandran number (\mathcal{R}) – that combines the values ϕ and ψ to produce a structurally meaningful number. This number depends on the fact that structural features of the backbone (e.g., radius of gyration) vary least when one slices through the *trans*

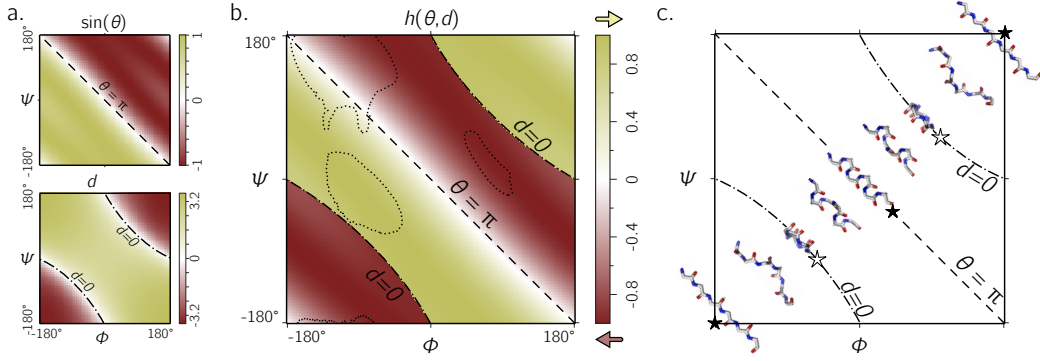


Figure 5. The chirality of an ordered *trans* peptide within the Ramachandran plot. Panel (a) displays the relationship between backbone parameters (ϕ, ψ) and the associated helix parameters of curvature $\sin(\theta)$ (top; Eqn. 1) and pitch d (bottom; Eqn. 2). The boundaries, $\theta = \pi$ (‘ $--$ ’) and $d = 0$ (‘ $- -$ ’), correspond to backbones that are equally flat, but which are respectively optimally extended and curved (see discussion in text). As shown in Fig. 3, the handedness of a helix is a function of these two variables (h ; Eqn. 10). Panel (b) is a map of backbone chirality (h) as a function of ϕ and ψ . This map shows that the naïve expectation of handedness in a Ramachandran plot (Fig. 1d) is inaccurate. Interestingly, our naïve expectations would be upheld if one were only to have sampled regions of the Ramachandran plot dominated by known proteins (a; regions enclosed by ‘ $....$ ’ indicate 90% occupancy). An example of the behavior of one ‘slice’ of (b) is shown in (c). Each snapshot represents a peptide backbone that is either in a distinct region of handedness or at a boundary.

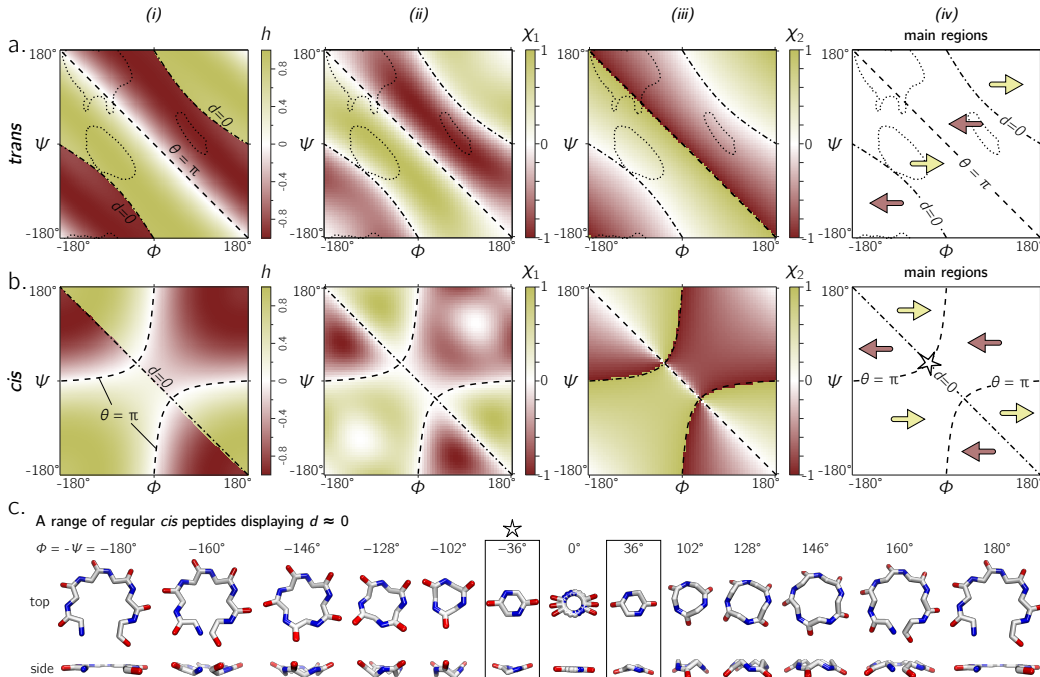


Figure 6. Panels (a) and (b) describe the handedness of backbone twists whose amide dihedral angles are *trans* ($\omega = \pi$) and *cis* ($\omega = 0$), respectively. Column (i) describes handedness calculated using h (Eqn. 10), which does not require structures to be computationally generated. Columns (ii) and (iii) respectively show vector-based estimates of backbone handedness – χ_1 (Eqn. 11) and χ_2 (Eqn. 12) – which are calculated from computationally generated peptides (see Methods). Regions of left- and right-handedness are identical for all measures (i–iii). This general map of how handedness is distributed within the Ramachandran plot is shown in (iv). Finally, Panel (c) displays a range of regular *cis* peptide backbones with $d \approx 0$. As explained by Fig. 4, $d = 0$ indicates a flatness of the peptide perpendicular to the helical axis, which results in peptides that close in on themselves at varying radii. Interestingly, a point in the Ramachandran plot exists exclusively for *cis* peptides, where $d = 0$ and $\theta = \pi$: $\phi = -\psi = \pm 36^\circ$ [\star in Panels(b)–(iv) and (c)].

262 Ramachandran plot along negative-sloping lines that conserve $\phi + \psi$ (Ho *et al.*, 2003; Zacharias and
263 Knapp, 2013; Mannige *et al.*, 2016). Interestingly, θ follows that trend too, which – in combination with
264 the fact that regions of the Ramachandran plot are sparse (Mannige *et al.*, 2016) – means that θ and its
265 derivatives (e.g., h) are *universal* Ramachandran numbers. The universality arises from the fact that *cis*
266 Ramachandran plots do *not* conserve structure along lines that conserve $\phi + \psi$ (and so \mathcal{R} only works for
267 *trans* backbones), yet any two backbones with nearly identical θ 's will also be conserved in structure (see,
268 e.g., Fig. 5a, top). This feature of θ will be true irrespective of the nature of the amide dihedral angle ω
269 (Eqn. 1).

270 **Handedness of *trans* backbones**

271 Fig. 5a describes the behavior of d and $\sin(\theta)$ as a function of ϕ and ψ (assuming an all-*trans* backbone;
272 $\omega = \pi$ or 180°). Fig. 5b describes the behavior of handedness (h ; Eqn. 10) as a function of ϕ and ψ .
273 This map is a complete description of the handedness of an all-*trans* (regular) peptide backbone. Fig. 5c
274 describes some structures at various regions within the plot. As discussed above (Fig. 4), $d = 0$ (‘ \star ’)
275 indicates that each residue is at the same ‘altitude’, i.e., the helix is perfectly flat and maximally curved
276 (at that particular θ). Note that any path on the Ramachandran plot that transitions from negative to
277 positive d will encounter an infinitesimal region in its path that is $d = 0$: it therefore appears as a sharp
278 transition from one handedness to the other. When $\theta = \pi$, then the backbone is also flat (see ‘ \star ’ in
279 Fig. 5c); however, atoms of the same type lie in a single plane that is perpendicular to the helical axis
280 (Fig. 4). In short, within the Ramachandran plot, $d = 0$ (‘ $- -$ ’) and $h = \pi$ (‘ $--$ ’) code for *flat* backbones
281 that are respectively either optimally curved (at a given θ) or optimally extended (at a given d). A future
282 report will discuss how these simple rules may be combined to make conjectures about novel secondary
283 and tertiary structures.

284 Fig. 6a shows that the equation for h match other metrics for handedness, as interpreted by other
285 metrics for chirality (Kwiecińska and Cieplak, 2005; Kabsch and Sander, 1983; Gruziel *et al.*, 2013). In
286 particular, Fig. 6a displays the Ramachandran plot colored by h [(i); Eqn. 10] next to estimates calculated
287 using χ_1 [(ii); Eqn. 11] and χ_2 [(iii); Eqn. 12]. Each panel describes identical regions of left- and
288 right-handedness, which is shown as a cartoon in (iv). However, given that χ_1 and χ_2 are estimates of
289 chirality and not backbone handedness, their exact values differ from the primary metric for handedness
290 (h) provided here.

291 **Handedness of *cis* backbones**

292 In the same vein as Fig. 6a, Fig. 6b displays h , χ_1 and χ_2 as a function of ϕ and ψ for all-*cis* backbones.
293 This appears to be the first complete description of chirality of an all-*cis* backbone ($\omega = 0$). Interestingly,
294 the boundaries for $d = 0$ and $\theta = \pi$ switch in *cis* backbones, with the -ve diagonal and curved boundaries
295 being caused by d and θ , respectively. Additionally, Fig. 6a reiterates the idea that *cis* peptides are quite
296 different when compared to *trans* peptides: the regions and boundaries of left- and right-handedness
297 within the Ramachandran plot differ for *cis* versus *trans*. Finally, points on the *cis* map ($\phi = \pm 36^\circ$,
298 $\psi = \mp 36^\circ$) exist where $d = 0$ and $\theta = \pi$. An example of this, along with other $d = 0$ configurations, is
299 shown in Fig. 6c for a six-residue peptide.

300 At first, this appears to be contradiction, because $d = 0$ indicates the most curved backbone at a fixed
301 θ , and $\theta = \pi$ indicates the most linear backbone at a fixed d . Of course, this structure would only be
302 possible for cyclic peptides with length two, given that any peptoid of length greater than two would
303 result in many overlapping atoms. However, such a structure (one with $d = 0$ and $\theta = \pi$) is not possible
304 in *trans* peptides, even in theory, because the boundaries associated with $d = 0$ and $\theta = \pi$ do not intersect
305 (Fig. 6a); this is also evident in Fig. 4, where *trans* peptides are shown to not occupy regions of $[d, \theta] =$
306 $[0, \pi]$, while *cis* peptides do.

307 **How does the amide backbone (ω) change the chirality landscape?**

308 So far, only discrete values for ω are discussed (either *cis* or *trans* peptides respectively corresponding
309 to $\omega = 0$ and π). The picture that arises is that our naïve picture of chirality – that the -ve diagonal
310 separates the right-twisting backbones from the left-twisting backbones (Fig. 1d) is wrong. In fact, the
311 Ramachandran plots for both *cis* and *trans* backbones describe not two but four regions of distinct chirality
312 (Fig. 6). However, deviations from $\omega = 0$ or π are evident in the Protein Databank; see, e.g., discussions
313 by Imrota *et al.* (2011). This raises the question of how does varying ω change the landscape? Fig. 7

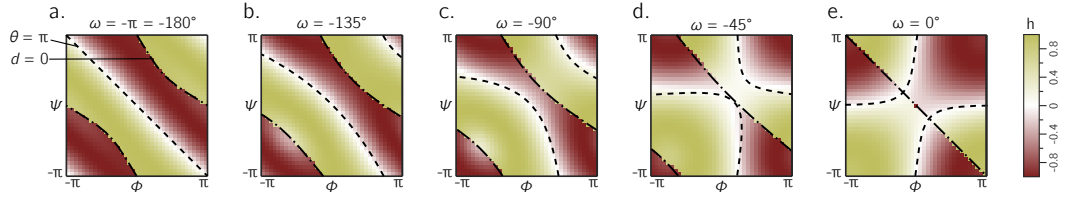


Figure 7. The landscape of backbone chirality as a function of amide dihedral angle ω . As ω is changed, the features of the landscape smoothly transform from the landscapes of $\omega = \pm\pi$ to $\omega = 0$. For all values of ω , it is evident that the naïve view of chirality (Fig. 1d) is wrong: at least four distinct regions of chirality [separated by boundaries $d = 0$ and $\sin(\theta) = \pi$] are evident in each scenario. Although only five snapshots (values of ω) are shown, all integer values of ω were tested, which corroborates the fact that the naïve view of backbone handedness (Fig. 1d) is universally incorrect.

describes some Ramachandran plots that show chirality in terms of varying values for ω . Fig. 7 shows that our naïve expectations of handedness (Fig. 1d) is too simple, irrespective of amide dihedral angle.

[-π,π] or [0,2π]: which frame of reference to use?

In structural biology, ϕ and ψ within the Ramachandran plot has been historically set to range between the values $[-\pi, \pi]$ radians [see, e.g., textbooks by Berg *et al.* (2010) and Alberts *et al.* (2002)]. However, Ramachandran *et al.* (1963) had originally used the range of $[0, 2\pi]$. Today, the range $[-\pi, \pi]$ is used predominantly by structural biologists (Laskowski *et al.*, 1993; Laskowski, 2003; Zacharias and Knapp, 2013), while some have turned to $[0, 2\pi]$ as the norm (Némethy *et al.*, 1966; Voelz *et al.*, 2011).

Given the periodicity of the Ramachandran plot, these differences do not make significant difference scientifically; however the value of the Ramachandran plot is undeniably relative to its boundaries: it is a map of important features of proteins relative to the various regions, quadrants, and diagonals in the map [see, e.g., discussions by Beck *et al.* (2008)]. The Ramachandran plot's value lies in being able to convey large amounts of information in easy to read logo- or picto-grams. For that reason, switching the map from one range to another means that two norms and two types of scientists will not be able to converse as seamlessly.

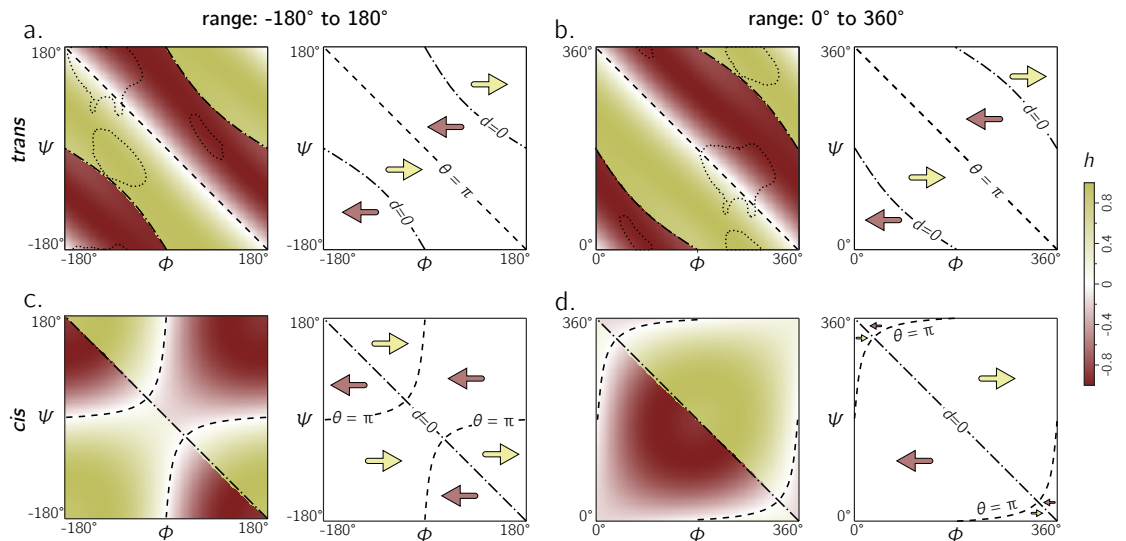


Figure 8. Each panel describes handedness data (right) and boundaries (left). Both frames of references $[-\pi, \dots, \pi]$ and $[0, \dots, 2\pi]$ yield similar trends for *trans* backbones (a,b); however, for *cis* backbones, the latter frame of reference (d) appears to more neatly apportion the handedness of the backbone rather than the traditional frame of reference (c). As in Figs. 5 and 6, ‘ $--$ ’ and ‘ $-.-$ ’ respectively correspond to boundaries defined by $\theta = \pi$ and $d = 0$. Also, regions bound by dotted contours indicate dominant regions within which proteins reside ($p = 0.9$).

Key: left-handed right-handed peptide occupancy (90%) regions within a Ramachandran plot (*trans*)

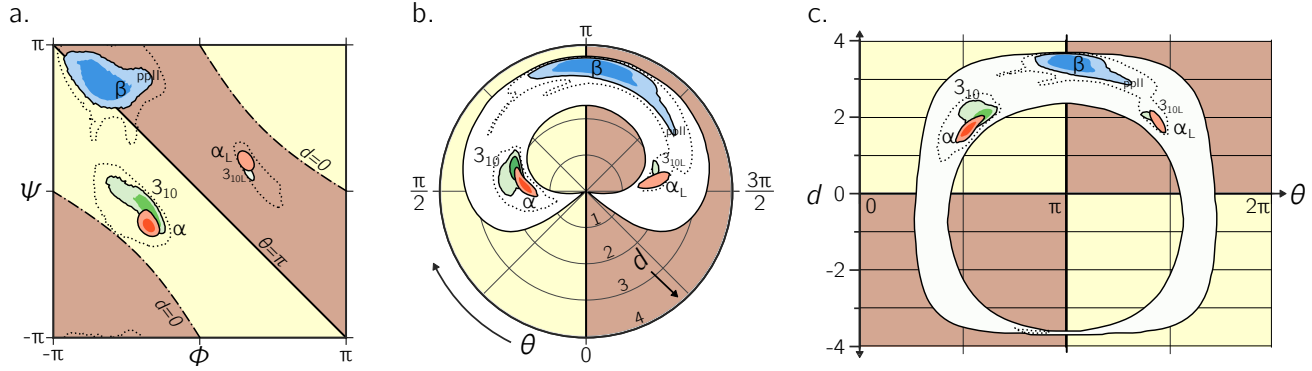


Figure 9. Alternative representations of the Ramachandran plot. While the Ramachandran plot is useful to map characteristics of secondary structures (a), it is not intuitive. For example, the relationship between the Ramachandran parameters (ϕ , ψ) and the handedness of a backbone is not obvious (see, e.g., the non-obvious distribution of left- and right-handed peptides as a function of ϕ and ψ). For this reason, Zacharias and Knapp (2013) introduced a graphical format involving the helical parameters d and θ in polar coordinate space (b), where the regions of left- and right-handedness are obvious [their format differs from (b) in that their θ increases in counter-clockwise fashion]. Panel (c), which is an extension of Fig. 4, introduces another graphical representation of backbone degrees of freedom based on (θ, d) , but in Cartesian space. While both (b) and (c) are equally useful in understanding regions available to a protein, the text discusses some benefits of (c) as a universal map for exploring new conformations and secondary structures. Excepting the left-handed helices (α_L -, 3_{10L} -helices), each secondary structure has two contours signifying $p = 0.5$ and 0.8 .

329 Therefore, the following question must arise: which range $[-\pi, \pi]$ or $[0, 2\pi]$ – is able to convey
 330 more information with the least amount of effort? Fig. 8 shows the behavior of a *trans* backbone (a,b) and
 331 *cis* backbone (c,d) in the two frames of reference. From (a) and (b) it is evident that general trends in
 332 the map for *trans* backbones remain the same in both frames of reference: the negative diagonal ($\sigma = \pi$)
 333 locally separates right-handed regions from left-handed regions, while the curved line ($d = 0$) – which
 334 also separates handedness – also appears to be in generally the same regions (albeit inverted in curvature).
 335 The *cis* backbones, however, look dramatically different in the two frames of reference: the range $[-\pi, \pi]$
 336 separates handedness in a more complicated manner (c), while, for the most part, the -ve diagonal appears
 337 to meaningfully separate handedness when the plot ranges from 0 to 2π (d). For this reason, purely when
 338 looking at handedness, and especially in the case of *cis* backbones, the Ramachandran plot that ranges
 339 between 0 and 2π appears to be more meaningful.

340 **A universal alternative to the Ramachandran plot**

341 While the Ramachandran plot is useful enough to earn a place in undergraduate-level biology textbooks,
 342 as discussed throughout this report, it is not easy to estimate features of a peptide backbone just from its
 343 (ϕ , ψ) angles (Fig. 9a). This prompted Zacharias and Knapp (2013) to introduce a new representation
 344 for backbone degrees of freedom in the form of a polar graph. In this polar representation, the θ is the
 345 angular coordinate (azimuth) and d is the radial coordinate. An example of one such representation is
 346 shown in Fig. 9b, with the direction of increasing θ reversed (compared to the cited report) to maintain
 347 relative positions of secondary structures within the Ramachandran plot (Fig. 9a). Zacharias and Knapp
 348 (2013) stated an additional reason for the introduction of the polar representation (Fig. 9b): θ , which is an
 349 angle and therefore periodic, can remain periodic as the angular coordinate in the graph.

350 However, the format proposed by Zacharias and Knapp (2013) (Fig. 9b) is incomplete for a few
 351 reasons: 1) $d < 0$ peptides (the bottom-left and top-right regions of Fig. 5a, bottom) will never be observed
 352 in this map since only structures with $d \geq 0$ are allowed; 2) all peptides with $d = 0$ (marked by ‘- -’
 353 in every preceding Ramachandran plot) will be compressed into one point at the center, even though
 354 Fig. 6c shows a range of legitimate $d = 0$ conformations); 3) while the graph is θ -periodic, the values for
 355 θ in peptides are constrained within one $[0, 2\pi]$ period (peptides range between $\theta = \pi/4$ and $2\pi - \pi/4$;
 356 vertical dotted lines in Fig. 4); i.e., periodicity in θ is not required for the faithful representation of
 357 peptides. Fortunately, even though this system is not universal (again, since $d < 0$ structures are not

358 accommodated), most conformations in globular proteins display positive d , and so the representation
359 presented by Zacharias and Knapp (2013) is a reasonable one for most proteins with known structure.

360 Interestingly, Fig. 9c – which arranges the parameters θ and d along Cartesian axes – serves as both a
361 universal *and* intuitive map for peptide backbone geometry. This is because: 1) as shown in Fig. 4, such
362 maps reveal a wealth of information about the peptide backbone, 2) both positive and negative values of d
363 are allowed (compared to Fig. 9b), due to the shift in the coordinate system from polar to Cartesian, and 3)
364 this format accommodates *every* type of peptide conformation: any peptide (or its mimic) has a place in
365 this map irrespective of whether the amide backbone is *cis* or *trans* or any other value; additionally, if the
366 backbone is distorted, such distortions can also be accounted for since d and θ includes such distortions
367 (Eqns. 1 and 2). This is impossible to do using a single Ramachandran plot without making sweeping
368 assumptions about backbone parameters that are not ϕ and ψ . The (θ, d) plot opens up the possibility for
369 a new, intuitive, and *universal* kind of graphical representation as a supplement to the Ramachandran plot.
370

371 **A departure from perfect regularity**

372 So far, this report has focused on *simple* regular backbone conformations, i.e., those that are formed from
373 the same ϕ and ψ angles repeated along the backbone. This is particularly because a simple and visually
374 intuitive correspondence exists between a regular backbone (described by myriad internal coordinates)
375 and a helix that is described simply by (d, θ, ρ_i) . This simple correspondence allows for an intuitive
376 understanding as to how to envision regular backbones as a function of d and θ (Figs. 3 and 4). There is a
377 possibility that d and θ are useful even in isolation, when the unreasonable constraint of perfect backbone
378 regularity is lifted. An example of such a departure from regularity follows.

379 Some secondary structures are characterized by the regular combination of two or more sets of (ϕ, ψ)
380 pairs (Pauling and Corey, 1951b,a; Armen *et al.*, 2004; Daggett, 2006; Hayward and Milner-White,
381 2008; Mannige *et al.*, 2015, 2016). For example, the Σ -strand is constructed by alternating between
382 two backbone states $(\phi, \psi, \omega) = (-A, B, 180^\circ)$ and $(-B, A, 180^\circ)$, where $A \approx 120$ and $B \approx 90$ [Fig. 4h in
383 Mannige *et al.* (2015)]. It was found that the two states are similar in the extent to which the backbone
384 twists, but opposite in handedness, which allows for these secondary structures to remain linear, albeit in a
385 meandering way (Mannige *et al.*, 2015). Eqn. 10 also describes these two states as opposite in handedness
386 and similar in twist extent: the h for the two states are -0.34 and 0.51 , respectively (the difference in
387 magnitude is within the range of the standard deviation in h [0.391] for the β -sheet). Similarly, the α -sheet
388 proposed by Pauling and Corey (1951a) is constructed by alternating between $\alpha_{(D)}$ and α_L backbone
389 states, yet this motif is linear because each state describes equal but opposite handedness $h = \pm 0.41$.
390 These points raise the possibility that, even in the absence of perfect backbone regularity, the values d and
391 θ may be considered to be residue-specific properties that may be combined to readily provide insights
392 about higher order structures.

393 CONCLUSIONS

394 This report introduces a metric for backbone handedness (h) that is based on modeling the backbone as
395 a helix [Fig. 2; Miyazawa (1961)]. In particular, h , which is a combination of the helical parameters
396 θ (angular displacement) and d (vertical displacement), ranges from -1 and 1, and is negative (or
397 positive) when the backbone twist is left(or right)-handed (with larger values indicating greater extent of
398 twistedness). This metric (h) was used to characterize every regular backbone's twist, via Ramachandran
399 plots, for both *cis* and *trans* peptides. In doing so, this report dispels a naïve view of handedness (Fig. 1d),
400 which states that backbone handedness in the Ramachandran plot is separated by the negative-sloped (-ve)
401 diagonal. Interestingly, the reason for the naïve view makes sense when considering only *trans* peptides:
402 the -ve diagonal ('--' in Figs. 5a) separates *D* and *L* twists if one considers only the regions dominantly
403 occupied by structured proteins ('....' in Figs. 5a). Plotting the backbone handedness (h) in the common
404 frames of reference $-\phi, \psi \in [-\pi, \pi]$ and $[0, 2\pi]$ – indicates that the less commonly used frame $[0, 2\pi]$
405 may be more appropriate for interpreting *cis* backbones (Fig. 8).

406 The behavior of a backbone in *cis* and *trans* Ramachandran plots look dramatically different (Fig. 6),
407 and so scientists dealing with new structures having a combination of *cis* and *trans* backbones can not
408 use one Ramachandran plot to faithfully describe these structures. Interestingly, the parameters θ and d
409 combine all features (internal coordinates) of a contorting backbone, including the amide dihedral angle
410 ω , which means that (θ, d) can describe *any* peptide backbone, irrespective of ω . The Cartesian plot with

411 θ and d as the x- and y-axis, respectively, serves as a unique plot for *any* peptide backbone (Fig. 9), with
412 specific values and boundaries containing deep structural meaning (Fig. 4). These discussions, the author
413 hopes, clarify a number of concepts associated with the Ramachandran plot, while providing new insights
414 into how to interrogate the features of new protein and protein-like structures.

415 **ACKNOWLEDGMENTS**

416 RVM thanks Alana Canfield Mannige for her support and input.

417 **REFERENCES**

- 418 **Alberts B, Johnson A, Lewis J, Raff M, Roberts K, Walter P. 2002.** Molecular biology of the cell.
419 new york: Garland science; 2002. *Classic textbook now in its 5th Edition* .
- 420 **Armen RS, DeMarco ML, Alonso DO, Daggett V. 2004.** Pauling and corey's α -pleated sheet structure
421 may define the prefibrillar amyloidogenic intermediate in amyloid disease. *Proceedings of the National
422 Academy of Sciences of the United States of America* **101**(32):11622–11627.
- 423 **Beck DA, Alonso DO, Inoyama D, Daggett V. 2008.** The intrinsic conformational propensities of the
424 20 naturally occurring amino acids and reflection of these propensities in proteins. *Proceedings of the
425 National Academy of Sciences* **105**(34):12259–12264.
- 426 **Bentley R. 2010.** Chiral: a confusing etymology. *Chirality* **22**(1):1–2.
- 427 **Berg JM, Tymoczko JL, Stryer L. 2010.** *Biochemistry, International Edition*. WH Freeman & Co.,
428 New York, 7 edition.
- 429 **Berman HM, Westbrook J, Feng Z, Gilliland G, Bhat T, Weissig H, Shindyalov IN, Bourne PE.**
430 2000. The protein data bank. *Nucleic acids research* **28**(1):235–242.
- 431 **Bragg L, Kendrew JC, Perutz MF. 1950.** Polypeptide chain configurations in crystalline proteins. *Pro-
432 ceedings of the Royal Society of London Series A Mathematical and Physical Sciences* **203**(1074):321–
433 357.
- 434 **Chothia C, Hubbard T, Brenner S, Barns H, Murzin A. 1997.** Protein folds in the all-beta and
435 all-alpha classes. *Annu Rev Biophys Biomol Struct* **26**:597–627.
- 436 **Cock P, Antao T, Chang J, Chapman B, Cox C, Dalke A, Friedberg I, Hamelryck T, Kauff F,
437 Wilczynski B, de Hoon M. 2009.** Biopython: freely available python tools for computational molecular
438 biology and bioinformatics. *Bioinformatics* **25**(11):1422–1423.
- 439 **Cooper GM, Hausman RE. 2013.** *The Cell: A Molecular Approach*. Sinauer Associates, Inc., Sunderland,
440 MA, 6 edition.
- 441 **Cross L, Klyne W. 2013.** *Rules for the Nomenclature of Organic Chemistry: Section E: Stereochemistry
442 (Recommendations 1974)*. Elsevier.
- 443 **Daggett V. 2006.** α -sheet: the toxic conformer in amyloid diseases? *Accounts of chemical research*
444 **39**(9):594–602.
- 445 **Eisenberg D. 2003.** The discovery of the α -helix and β -sheet, the principal structural features of proteins.
446 *Proceedings of the National Academy of Sciences* **100**(20):11207–11210.
- 447 **Esposito L, Balasco N, De Simone A, Berisio R, Vitagliano L. 2013.** Interplay between peptide bond
448 geometrical parameters in nonglobular structural contexts. *BioMed research international* **2013**.
- 449 **Ferrarini A, Nordio PL. 1998.** On the assessment of molecular chirality. *Journal of the Chemical
450 Society, Perkin Transactions 2* (2):455–460.
- 451 **Fox NK, Brenner SE, Chandonia JM. 2014.** Scope: Structural classification of proteins—extended,
452 integrating scop and astral data and classification of new structures. *Nucleic Acids Res* **42**(Database
453 issue):D304–D309. doi:10.1093/nar/gkt1240.
- 454 **Frishman D, Argos P. 1995.** Knowledge-based protein secondary structure assignment. *Proteins:
455 Structure, Function, and Bioinformatics* **23**(4):566–579.
- 456 **Gold V, Loening K, McNaught A, Shemi P. 1997.** Iupac compendium of chemical terminology.
457 *Blackwell Science, Oxford* .
- 458 **Gorske BC, Mumford EM, Conry RR. 2016.** Tandem incorporation of enantiomeric residues engenders
459 discrete peptoid structures. *Organic letters* .
- 460 **Gruziel M, Dzwolak W, Szymczak P. 2013.** Chirality inversions in self-assembly of fibrillar superstruc-
461 tures: a computational study. *Soft Matter* **9**(33):8005–8013.

- 462 **Harris AB, Kamien RD, Lubensky TC.** 1999. Molecular chirality and chiral parameters. *Reviews of*
463 *Modern Physics* **71**(5):1745.
- 464 **Hayward S, Milner-White EJ.** 2008. The geometry of α -sheet: Implications for its possible function as
465 amyloid precursor in proteins. *Proteins: Structure, Function, and Bioinformatics* **71**(1):415–425.
- 466 **Ho BK, Thomas A, Brasseur R.** 2003. Revisiting the ramachandran plot: Hard-sphere repulsion,
467 electrostatics, and h-bonding in the α -helix. *Protein Science* **12**(11):2508–2522.
- 468 **Hooft RW, Sander C, Vriend G.** 1997. Objectively judging the quality of a protein structure from a
469 ramachandran plot. *Computer applications in the biosciences: CABIOS* **13**(4):425–430.
- 470 **Iakoucheva LM, Brown CJ, Lawson JD, Obradović Z, Dunker AK.** 2002. Intrinsic disorder in
471 cell-signaling and cancer-associated proteins. *Journal of molecular biology* **323**(3):573–584.
- 472 **Improta R, Vitagliano L, Esposito L.** 2011. Peptide bond distortions from planarity: new insights from
473 quantum mechanical calculations and peptide/protein crystal structures. *PLoS One* **6**(9):e24533.
- 474 **Improta R, Vitagliano L, Esposito L.** 2015a. Bond distances in polypeptide backbones depend on the
475 local conformation. *Acta Crystallographica Section D: Biological Crystallography* **71**(6):1272–1283.
- 476 **Improta R, Vitagliano L, Esposito L.** 2015b. The determinants of bond angle variability in pro-
477 tein/peptide backbones: A comprehensive statistical/quantum mechanics analysis. *Proteins: Structure,*
478 *Function, and Bioinformatics* **83**(11):1973–1986.
- 479 **Kabsch W, Sander C.** 1983. Dictionary of protein secondary structure: pattern recognition of hydrogen-
480 bonded and geometrical features. *Biopolymers* **22**(12):2577–2637. doi:10.1002/bip.360221211.
- 481 **Kwiecińska JI, Cieplak M.** 2005. Chirality and protein folding. *Journal of Physics: Condensed Matter*
482 **17**(18):S1565.
- 483 **Laskowski RA.** 2003. Structural quality assurance. *Structural Bioinformatics, Volume 44* pages 273–303.
- 484 **Laskowski RA, MacArthur MW, Moss DS, Thornton JM.** 1993. Procheck: a program to check the
485 stereochemical quality of protein structures. *Journal of applied crystallography* **26**(2):283–291.
- 486 **Linderstrøm-Lang KU.** 1952. *Lane Medical Lectures: proteins and enzymes*, volume 6. Stanford
487 University Press.
- 488 **Mannige RV.** 2014. Dynamic new world: Refining our view of protein structure, function and evolution.
489 *Proteomes* **2**(1):128–153.
- 490 **Mannige RV, Haxton TK, Proulx C, Robertson EJ, Battigelli A, Butterfoss GL, Zuckermann RN,**
491 **Whitelam S.** 2015. Peptoid nanosheets exhibit a new secondary structure motif. *Nature* **526**:415–420.
- 492 **Mannige RV, Kundu J, Whitelam S.** 2016. The Ramachandran number: an order parameter for protein
493 geometry. *PLoS One* **11**(8):e0160023.
- 494 **Mirijanian DT, Mannige RV, Zuckermann RN, Whitelam S.** 2014. Development and use of an
495 atomistic charmm-based forcefield for peptoid simulation. *J Comput Chem* **35**(5):360–370.
- 496 **Mislow K.** 2002. Stereochemical terminology and its discontents. *Chirality* **14**(2-3):126–134.
- 497 **Miyazawa T.** 1961. Molecular vibrations and structure of high polymers. ii. helical parameters of infinite
498 polymer chains as functions of bond lengths, bond angles, and internal rotation angles. *Journal of*
499 *Polymer Science* **55**(161):215–231.
- 500 **Neal MP, Solymosi M, Wilson MR, Earl DJ.** 2003. Helical twisting power and scaled chiral indices.
501 *The Journal of chemical physics* **119**(6):3567–3573.
- 502 **Némethy G, Leach S, Scheraga HA.** 1966. The influence of amino acid side chains on the free energy
503 of helix-coil transitions1. *The Journal of Physical Chemistry* **70**(4):998–1004.
- 504 **Orosz F, Ovádi J.** 2011. Proteins without 3d structure: definition, detection and beyond. *Bioinformatics*
505 **27**(11):1449–1454.
- 506 **Osipov M, Pickup B, Dunmur D.** 1995. A new twist to molecular chirality: intrinsic chirality indices.
507 *Molecular Physics* **84**(6):1193–1206.
- 508 **Pauling L, Corey RB.** 1951a. Configurations of polypeptide chains with favored orientations around
509 single bonds: two new pleated sheets. *Proceedings of the National Academy of Sciences of the United*
510 *States of America* **37**(11):729.
- 511 **Pauling L, Corey RB.** 1951b. The pleated sheet, a new layer configuration of polypeptide chains.
512 *Proceedings of the National Academy of Sciences of the United States of America* **37**(5):251.
- 513 **Pauling L, Corey RB, Branson HR.** 1951. The structure of proteins: two hydrogen-bonded helical
514 configurations of the polypeptide chain. *Proceedings of the National Academy of Sciences* **37**(4):205–
515 211.
- 516 **Ramachandran G, Ramakrishnan C, Sasisekharan V.** 1963. Stereochemistry of polypeptide chain

- 517 configurations. *Journal of molecular biology* **7**(1):95–99.
- 518 **Robertson EJ, Battigelli A, Proulx C, Mannige RV, Haxton TK, Yun L, Whitelam S, Zuckermann**
519 **RN. 2016.** Design, synthesis, assembly, and engineering of peptoid nanosheets. *Accounts of chemical*
520 *research* **49**(3):379–389.
- 521 **Shimanouchi T, Mizushima Si. 1955.** On the helical configuration of a polymer chain. *The Journal of*
522 *Chemical Physics* **23**(4):707–711.
- 523 **Solymosi M, Low RJ, Grayson M, Neal MP. 2002.** A generalized scaling of a chiral index for molecules.
524 *The Journal of chemical physics* **116**(22):9875–9881.
- 525 **Sun J, Zuckermann RN. 2013.** Peptoid polymers: a highly designable bioinspired material. *ACS Nano*
526 **7**(6):4715–4732. doi:10.1021/nn4015714.
- 527 **Testa B. 2013.** Organic stereochemistry. part 2. *Helvetica Chimica Acta* **96**(2):159–188.
- 528 **Tien MZ, Sydkova DK, Meyer AG, Wilke CO. 2013.** Peptidebuilder: A simple python library to
529 generate model peptides. *PeerJ* **1**:e80.
- 530 **Van Der Walt S, Colbert SC, Varoquaux G. 2011.** The numpy array: a structure for efficient numerical
531 computation. *Computing in Science & Engineering* **13**(2):22–30.
- 532 **Voelz VA, Dill KA, Chorny I. 2011.** Peptoid conformational free energy landscapes from implicit-solvent
533 molecular simulations in amber. *Peptide Science* **96**(5):639–650.
- 534 **Wallentin CJ, Orentas E, Wärnmark K, Wendt OF. 2009.** Chirality, a never-ending source of con-
535 fusion. *Zeitschrift für Kristallographie International journal for structural, physical, and chemical*
536 *aspects of crystalline materials* **224**(12):607–608.
- 537 **Ward JJ, Sodhi JS, McGuffin LJ, Buxton BF, Jones DT. 2004.** Prediction and functional analysis of
538 native disorder in proteins from the three kingdoms of life. *J Mol Biol* **337**(3):635–645.
- 539 **Zacharias J, Knapp EW. 2013.** Geometry motivated alternative view on local protein backbone
540 structures. *Protein Science* **22**(11):1669–1674.